Molecular Dynamics Simulations of the Melting of 1,3,3-Trinitroazetidine

Paras M. Agrawal[†]

Department of Chemistry, Oklahoma State University, Stillwater, Oklahoma 74078

Betsy M. Rice

U.S. Army Research Laboratory, AMSRL-ARL-WM-BD, Weapons and Materials Research Directorate, Aberdeen Proving Ground, Maryland 21005-5069

Lianqing Zheng, Gustavo F. Velardez, and Donald L. Thompson*

Department of Chemistry, University of Missouri—Columbia, Columbia, Missouri 65211

Received: November 18, 2005; In Final Form: January 9, 2006

Physical properties of condensed-phase 1,3,3-trinitroazetidine (TNAZ) have been computed with molecular dynamics (MD) and a nonreactive, fully flexible force field formulated by combining the intramolecular interactions obtained from the Generalized AMBER Force Field and the rigid-molecule force field developed by Sorescu−Rice−Thompson [*J. Phys. Chem. B* **1997**, *101*, 798] (AMBER-SRT). The results are compared with MD calculations, using the AMBER force field. The predicted densities of crystalline TNAZ from both force fields are about 10% lower than the experimental value. The calculated thermodynamic melting point at 1 atm from the AMBER-SRT force field is 390 K, in good agreement with the measured value of 374 K, while the AMBER force field predicts a thermodynamic melting point of 462 K. The lattice parameters and the molecular and crystal structures calculated with the AMBER-SRT force field are in excellent agreement with experiment. Simulations with the AMBER-SRT force field were also used to generate the isotherm of TNAZ up to 4 GPa and the bulk modulus and its pressure derivative.

I. Introduction

We report the results of molecular dynamics (MD) simulations of 1,3,3-trinitroazetidine (TNAZ) using two force fields. The main purpose of this work was to assess the feasibility of using a standard force field (we have chosen to use AMBER[1]) to describe the physical properties, including melting, of nitro and nitramine solids, which are commonly used as energetic materials. It is not possible to select a truly stereotypical system for nitro and nitramine energetic materials because they include a wide diversity of compounds (e.g., acyclic, mono- and polycyclic, aliphatic, and aromatic). We have selected TNAZ because it is representative of some classes of nitro and nitramine energetic materials, e.g., it contains both nitramine and nitro groups. It has a four-member ring structure (see Figure 1) with 37 kcal/mol strain energy.[2] It is approximately 30% more energetic than TNT and at least 10% more than other cyclic nitramines such as RDX (1,3,5-hexahydro-1,3,5-*s*-triazine) and HMX (octahydro-1,3,5,7-tetranitro-1,3,5,7-tetraazacyclooctane).[3,4] The normal melting point is ∼101 °C and it is thermally stable up to ∼240 °C.[4] There are important differences in the various energetic molecules, but TNAZ possesses enough of the important traits that it is a suitable prototype for testing the feasibility of making use of standard force fields in MD simulations for predicting physical properties, particularly melting point, of energetic materials. We recognize that these force fields cannot necessarily be expected to be accurate for properties not considered in their development; nevertheless they provide a readily available starting point for developing the force fields needed for energetic materials. How they can be used for modeling properties of energetic materials is the focus of this study.

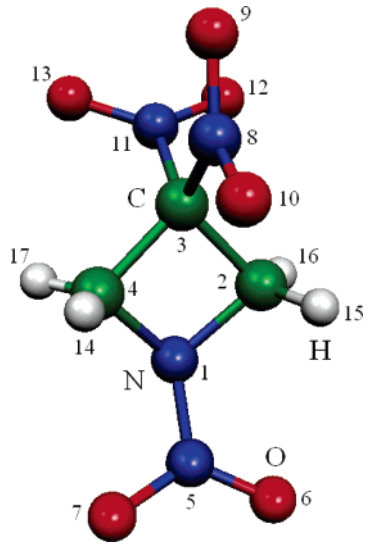

Figure 1. Molecular structure of TNAZ, with labels of atoms used in the discussion.

We present a fully flexible force field for TNAZ based on the Generalized AMBER Force Field (GAFF)[1] and the Sorescu−

* Address correspondence to this author.
[†] Present address: Department of Mechanical and Aerospace Engineering, Oklahoma State University, Stillwater, OK 74078.

10.1021/jp056690g CCC: $33.50
Published on Web 03/01/2006

Rice−Thompson (SRT) rigid-molecule force field.[5] The parameters for the intramolecular interactions are directly taken from the GAFF force field while we use the SRT potential for the intermolecular interactions. We perform MD simulations using this force field to compute several fundamental properties of TNAZ: density, crystal and molecular structure, lattice parameters, melting point, and isotherm.

We have reported a series of MD studies of the physical properties of organic and ionic materials, with an emphasis on energetic materials, using fully flexible empirical force fields. We have studied the solid and liquid properties and melting points of nitromethane,[6] ammonium dinitramide,[7] ammonium nitrate,[8] [emim][PF_6],[9] [patr][Br],[10] and dimethylnitramine.[11] Various force fields were used in these studies, including custom-designed[12] and general (e.g., AMBER and OPLS[13]) force fields. These studies suggest that general force fields such as AMBER and OPLS are sufficient to describe the ionic materials. This may be due to the relative strengths of the van der Waals and Coulombic forces in salts. Obtaining accurate force fields for molecular solids and liquids appears at this time to be a more difficult problem, based on a limited number of studies. We have developed a general force field formalism for CHNO solids assuming rigid molecules that accurately describes solid-state properties of a wide range of materials.[5,14,15] Of course, rigid-molecule models have limited applicability, and there is a real need to have completely realistic force fields for treating thermodynamic and dynamic processes.

Many of the force fields available for energetic materials have been specifically designed for particular compounds. We have developed such a model for nitromethane,[12] and have shown that it is highly accurate for predicting solid and liquid properties, including the solid-to-liquid transition.[6,12,16] The formulation and parametrization of such force fields require considerable effort. Thus, it is useful to explore the accuracy of using standard general intramolecular force fields with the rigid-molecule models that we have developed and tested. We would first like to know the accuracy of such models if applied without modifications, and then determine whether they could be improved for cases where they are not acceptably accurate. Along this test we report here the results of MD simulations of TNAZ using a force field constructed simply by adding the intramolecular interactions from AMBER to the SRT force field. We note that coupling a generic flexible-molecule force field with an existing rigid-molecule model is not expected to work well for floppy molecules, and point out that in the present case we have chosen a molecule that is not highly flexible. Furthermore, it is expected that MD simulations with this hybrid potential will predict smaller densities than those produced assuming the rigid-body terms only, since the inclusion of intramolecular motions in the dynamics should result in a volume increase. The SRT model[5] of the intermolecular terms, which was shown to reasonably predict densities of numerous CHNO crystals, was parametrized by fitting the density (and other properties) with rigid structures. Thus, it is expected that inclusion of the intramolecular terms will result in a poorer description of density than that obtained from rigid-body MD simulations.

II. Force Fields

A. AMBER Force Field. The potential energy in the AMBER force field is a sum of bond stretching, angle bending, dihedral torsions, van der Waals interactions, and electrostatic interactions:

$$E_{\text{total}} = \sum_{\text{bonds}} K_r(r - r_{\text{eq}})^2 + \sum_{\text{angles}} K_\theta(\theta - \theta_{\text{eq}})^2 + \sum_{\text{dihedrals}} \frac{V_n}{2}[1 + \cos(n\phi - \gamma)] + \sum_{i<j}\left[\left(\frac{A_{ij}}{R_{ij}^{12}} - \frac{B_{ij}}{R_{ij}^{6}}\right) + \frac{q_i q_j}{4\pi\epsilon_0 R_{ij}}\right] \quad (1)$$

where r, θ, ϕ, R_{ij}, and q_i are the bond length, bending angle, torsional angle, interatomic distance between atoms i and j, and partial charge of atom i, respectively; r_{eq}, θ_{eq}, K_r, and K_θ are the equilibrium bond length and bond angle and corresponding force constants for harmonic bond stretching and angle bending, respectively; V_n, n, and γ are the torsional barrier, periodicity, and phase offset, respectively; and A_{ij}, B_{ij}, and ϵ_0 are parameters in the Lennard-Jones potential and dielectric permittivity for vacuum, respectively. The r_{eq}, θ_{eq}, K_r, and K_θ values were adjusted by using ab initio calculations, crystal structures, and experimental normal-mode frequencies. The torsional angle parameters were obtained from ab initio calculations. Monte Carlo simulations were carried out to develop the van der Waals parameters to reproduce the densities and enthalpies of vaporization of the liquids. The parameters of these terms are taken from the GAFF force field in AMBER 7.[1] The parameters for the NNOO and CNOO torsions (improper dihedrals) are not available in AMBER and are set equal to that for ONOO from ref 17.

B. AMBER-SRT Force Field. The AMBER-SRT force field has the same functional form as the AMBER force field except that the van der Waals interactions are expressed by using Buckingham (exp-6) potential instead of the 12-6 Lennard-Jones potential:

$$E_{\text{vdw}} = \sum_{i<j}(A_{ij}\mathrm{e}^{-B_{ij}r_{ij}} - C_{ij}/r_{ij}^6) \quad (2)$$

The A_{ij}, B_{ij}, and C_{ij} parameters were determined through a combination of nonlinear least-squares fitting to observed crystal structures and lattice energies and trial-and-error adjustment.[5] The parameters in the intramolecular interactions are also taken from the GAFF of AMBER 7[1] and those of the van der Waals interactions are given in ref 5.

C. Partial Charges. The partial charges have been computed by fitting the quantum mechanically derived electrostatic potential over a large number of grid points by the method proposed by Breneman and Wiberg[18] incorporated in the Gaussian 98 package of programs[19] under the keyword CHELPG. The calculations were performed at the HF/6-31G** level on a single molecule with the structure corresponding to that in the crystal at ambient conditions.[20]

III. Computational Procedures

Two separate series of isothermal−isobaric (NPT-MD) simulations were performed. The first are standard NPT-MD simulations at $T = 300$ K, $P = 1$ atm, to establish the crystal structures for TNAZ at ambient conditions. The second are NPT-MD simulations in which the temperature is gradually increased during the simulations until the melting of the crystals occurs. The procedure for the gradual heating of the crystal is the same as that detailed in ref 6. In that work, thermodynamic quantities and internal energy distributions evaluated with this method of heating were calculated at selected temperatures during the heating process. These were then compared with simulated values at the same temperature, for which a temperature gradient was not applied. The thermodynamic quantities and fluctuations

are comparable, suggesting that this method of heating does not introduce aphysical effects into the thermodynamic quantities.

The Melchionna modification[21] of the Nosé−Hoover equations of motion is used to perform the NPT-MD simulations. The Nosé−Hoover thermostat and barostat relaxation times have been chosen as 2.0 and 5.0 ps, respectively. The equations of motion are integrated by using the Verlet leapfrog procedure[22] with a time step of 1.0 fs. The DL_POLY_2.0 molecular dynamics program[23] was used to perform all simulations. The cutoff distance for the intermolecular potential was set to 11.0 Å. Minimum image periodic boundary conditions were imposed in all dimensions during the simulations and long-range corrections to the energy and virial expressions were included. Long-range Coulombic interactions were handled by using Ewald's method.[22,24] Single-crystal neutron diffraction measurement shows that structure of crystalline TNAZ[20] belongs to the orthorhombic space group *Pbca* with eight molecules per unit cell at ambient conditions. In our calculations the simulation box consists of $4 \times 2 \times 2$ unit cells of TNAZ, which contains 128 molecules (2176 atoms).

The void-nucleated melting method as described by Agrawal et al.[6] was used to compute the thermodynamic melting point (T_m). To overcome the superheating effects in the MD simulations due to the absence of surface, molecules are randomly chosen for removal from the supercell to create voids. The melting is accomplished by the uniform gradual heating of the system as described in ref 6. In this method the value of the imposed temperature is increased at every time step by ΔT. Thus, the temperature T at the simulation time step n_s is related to the initial temperature T_0 of the lattice by

$$T = T_0 + (\Delta T) n_s \tag{3}$$

For most of the calculations, $\Delta T = 2.5 \times 10^{-4}$ K has been chosen. A few simulations have also been run with a lower rate ($\Delta T = 1.0 \times 10^{-4}$ K) but the results do not change. The melting of the system has been detected by monitoring the energy, density, and order parameter ζ as functions of temperature. At the phase-transition temperature, these parameters change abruptly.

The translational symmetry of the orthorhombic space group has been used to define and compute the order parameter ζ

$$\zeta = \frac{1}{8}\sum_{i=1}^{8}\zeta_i = \frac{1}{8}\sum_{i=1}^{8}\frac{1}{N_c}\left|\sum_{j=1}^{N_c}\exp(i\vec{k}_i\cdot\vec{r}_j)\right| \tag{4}$$

where ζ_i represents an order parameter defined for each of the eight symmetry-related molecules that occupy the unit cell, averaged over all unit cells N_c in the system. The vector $\vec{k}_i$ is defined as

$$\vec{k}_i = 2\pi(\vec{i}/a + \vec{j}/b + \vec{k}/c) \tag{5}$$

where a, b, and c denote the unit cell edge lengths. The vector $\vec{r}_j$ is the coordinate of the center of mass of the TNAZ molecule in the jth unit cell.

The isotherm of TNAZ at 300 K is predicted up to 4 GPa. We calculated the bulk modulus (B_0) and its pressure derivative (B_0') at ambient conditions by fitting the isotherm to the third-order Birch−Murnaghan equation:[25]

$$P(V) = \frac{3}{2}B_0\left[\left(\frac{V}{V_0}\right)^{-7/3} - \left(\frac{V}{V_0}\right)^{-5/3}\right]\left\{1 - \frac{3}{4}(4 - B_0')\left[\left(\frac{V}{V_0}\right)^{-2/3} - 1\right]\right\} \tag{6}$$

where V_0 is the volume at 1 atm.

TABLE 1: Summary of Calculated and Measured Physical Properties of Crystalline TNAZ: Density, Lattice Parameters, and Melting Points

	AMBER-SRT	AMBER	experiment[b]
density (g/cm^3)[a]	1.65	1.70	1.86
a (Å)[a]	6.031	6.076	5.733
b (Å)[a]	11.610	11.382	11.127
c (Å)[a]	22.028	21.737	21.496
α (deg)[a]	90.1	90.0	90.0
β (deg)[a]	90.0	90.0	90.0
γ (deg)[a]	90.2	90.0	90.0
T_s (K)	461	546	
T_m (K)	390[c]	462[d]	374[e]

[a] $T = 300$ K and $P = 1$ atm. [b] Archibald et al., ref 20. [c] Calculated by using the void-nucleated method. [d] Calculated from T_s by assuming the same amount of superheating as determined for the AMBER-SRT potential. [e] Sikder et al., ref 3.

IV. Results and Discussion

We first compare the properties of TNAZ calculated from MD simulations using the AMBER-SRT and AMBER potentials with experiment. A summary of the experimental and calculated crystallographic parameters and melting points for TNAZ predicted by both potentials is given in Table 1. Cell edges a, b, and c deviate from experiment by 5.2%, 4.3%, and 2.5%, respectively, using the AMBER-SRT potential, while the errors from the AMBER potential are 6.0%, 2.3%, and 1.1%, respectively. The calculated densities of crystalline TNAZ from the AMBER-SRT and AMBER potentials are 1.65 and 1.70 g/cm^3, respectively, about 11% and 8.6% lower than the measured value of 1.86 g/cm^3. Conversely, molecular packing (MP) calculations of TNAZ[26] with the rigid-body SRT model predict a value for the density that is only 1.3% larger than the experiment value. Since the MP calculations do not include thermal effects, this error should be considered an upper limit and would, barring anomalous thermal expansion behavior, be smaller. Additionally, the cell edges a, b, and c predicted in the MP study using the SRT potential deviate from experiment by 0.4%, −0.6%, and −1.1%. Thus, it is apparent that including intramolecular terms in the force field produces a substantial lowering of the predicted densities.

The AMBER-SRT potential predicts the melting point of a perfect TNAZ crystal (T_s) to be 461 K and a thermodynamic melting point (T_m) of 390 K, using the void-nucleated method (the details are further addressed below). This is in good agreement with the experimental value of 374 K. The T_s calculated from the AMBER potential is 546 K. Assuming that the ratio of T_m and T_s (T_m/T_s) is the same as the one from the AMBER-SRT potential, we estimate a T_m of 462 K using the AMBER potential, a significant difference from the measured value. Though the AMBER potential gives slightly better results of density and lattice parameters, the prediction of the melting point is much more accurate with the AMBER-SRT potential. Therefore, we present more detailed results only from the AMBER-SRT potential in the rest of this section.

Table 2 provides a comparison of averaged fractional center-of-mass coordinates and orientation Euler angles for the eight molecules in the unit cell with experimental values. The Euler angles for each molecule were determined from a rotational matrix that transforms the body-fixed coordinates of the molecules (with axes corresponding to the principal axes of inertia) to the reference frame of the molecule (i.e., the space-fixed coordinate system of the molecule, which has unit vectors along the Cartesian axes). The largest deviations of the components of the fractional coordinates from the experimental

TABLE 2: Orientational Parameters (center-of-mass fractionals and Euler angles[a]) and Molecular Structural Parameters for the Eight TNAZ Molecules in the Unit Cell[d]

	1			2			3			4		
	expt[b]	NPTMD[c]		expt[b]	NPTMD[c]		expt[b]	NPTMD[c]		expt[b]	NPTMD[c]	
sx	0.4057	0.4093	(0.0036)	0.0943	0.0889 [0.0907]	(−0.0054)	0.9057	0.8900 [0.9093]	(−0.0157)	0.5943	0.5874 [0.5907]	(−0.0069)
sy	0.2585	0.2331	(−0.0254)	0.7415	0.7200 [0.7669]	(−0.0215)	0.2415	0.2208 [0.2669]	(−0.0207)	0.7585	0.7324 [0.7331]	(−0.0261)
sz	0.1253	0.1261	(0.0008)	0.6253	0.6259 [0.6261]	(0.0006)	0.8747	0.8741 [0.8739]	(−0.0006)	0.3747	0.3737 [0.3739]	(−0.0010)
θ	3.2	−1.5	(−4.7)	−3.2	1.7 [1.5]	(4.9)	−3.2	1.6 [1.5]	(4.8)	3.2	−1.9 [−1.5]	(−5.1)
ϕ	80.9	83.2	(2.3)	80.9	83.3 [83.2]	(2.4)	99.1	96.9 [96.8]	(−2.2)	99.1	96.8 [96.8]	(−2.3)
ψ	44.1	51.8	(7.7)	−44.1	−45.5 [−51.8]	(−1.4)	44.1	51.0 [51.8]	(6.9)	−44.1	−44.4 [−51.8]	(−0.3)
	5			6			7			8		
	expt[b]	NPTMD[c]		expt[b]	NPTMD[c]		expt[b]	NPTMD[c]		expt[b]	NPTMD[c]	
sx	0.5943	0.5878 [0.5907]	(−0.0065)	0.9057	0.8803 [0.9093]	(−0.0254)	0.0943	0.0864 [0.0907]	(−0.0079)	0.4057	0.4119 [0.4093]	(0.0062)
sy	0.7415	0.7205 [0.7669]	(−0.0210)	0.2585	0.2331 [0.2331]	(−0.0254)	0.7585	0.7324 [0.7331]	(−0.0261)	0.2415	0.2206 [0.2669]	(−0.0209)
sz	0.8747	0.8739 [0.8739]	(−0.0008)	0.3747	0.3741 [0.3739]	(−0.0006)	0.1253	0.1261 [0.1261]	(0.0008)	0.6253	0.6263 [0.6261]	(0.0010)
θ	3.2	−1.2 [−1.5]	(−4.4)	−3.2	1.6 [1.5]	(4.8)	−3.2	1.4 [1.5]	(4.6)	3.2	−1.7 [−1.5]	(−4.9)
ϕ	80.9	83.5 [83.2]	(2.6)	80.9	83.3 [83.2]	(2.4)	99.1	96.8 [96.8]	(−2.3)	99.1	96.7 [96.8]	(−2.4)
ψ	44.1	52.4 [51.8]	(8.3)	−44.1	−44.7 [−51.8]	(−0.6)	44.1	49.6 [51.8]	(5.5)	−44.1	−44.7 [−51.8]	(−0.6)

[a] Units are in degrees. [b] Archibald et al., ref 20. [c] Values in parentheses are absolute differences from experimental values; values in square brackets are ideal orientational parameters based on the *Pbca* space group symmetry operators and the orientational parameters of molecule 1. [d] NPT-MD values are averaged over time and all unit cells within the 4 × 2 × 2 simulation cell.

values are within ∼0.026. This shows that the molecular centers of the eight molecules are in approximately the correct positions. The agreement of the orientational Euler angles with experiment is reasonably good; the largest deviations of the Euler angles θ, ϕ, and ψ from experiment are −5.1°, 2.6°, and 8.3°, respectively. We also compare averaged fractional coordinates and orientational Euler angles for the eight molecules in the unit cell with orientational parameters for a perfect crystal of TNAZ (also given in Table 2). A comparison of the averaged values with the "ideal" predictions indicates that the space group symmetry is fairly well maintained during the simulations.

The calculated C−C and C−N ring bond lengths are within 0.0035 Å of the experimental values. The deviation of the nonring covalent bonds in this molecule are somewhat larger (0.15, 0.09, and 0.1 Å for the C−H, N−N, and NO bonds, respectively). The calculated ring angles (CCC and CCN) are both within ∼10° of the experimental values, and the HCH and NCN angles are both within 7.4° of the experimental values. The CNN and nonring CCN angles differ from experiment by 5.4° and 1.8°, respectively. The nitramine- and nitro-ONO angles are within 1.7° and 4.2°, respectively, of the measured values.

Seven dihedral angles are used to describe the arrangement of the atoms or groups attached to the TNAZ ring; values are given for each of the molecules in the unit cell. The atom indices (see Figure 1) defining each dihedral angle are given in Table 3, and the calculated averages and experimental values are given in Table 4. The first dihedral angle τ_1 depicts the deviation from planarity of the four ring atoms. The predicted rings are all ∼7° closer to planarity than the experimental molecule. The tilt of the N−N bond relative to the ring atoms is given by dihedral angle τ_2, and is within 3.6° of experiment. Dihedral angles τ_3, τ_4, and τ_5 depict the rotation of the NO_2 groups about the N−N and two nonring C−N bonds; the orientation of the nitramine

TABLE 3: Specification of Atoms Used To Defined Various Dihedral Angles in TNAZ

	atom used to define thedihedral angle[a]			
dihedral angles	*i*	*j*	*k*	*l*
τ_1	3	2	4	1
τ_2	3	2	4	5
τ_3	2	4	7	6
τ_4	9	10	1	3
τ_5	2	4	13	12
τ_6	1	2	4	8
τ_7	1	2	4	11

[a] Atom labels are as defined in Figure 1.

NO_2 group is in better agreement with experiment than those attached to the carbon. Dihedral angles τ_4 and τ_5 denote the tilt of the two nonring C−N bonds relative to the ring and are within ∼7° and 4°, respectively, of experimental values. Overall, the lack of gross deviation in structural features of the calculated molecules and the reasonable adherence to the *Pbca* space group symmetry indicates that the contents of the predicted unit cell resemble the experimental counterpart. However, the changes in molecular structure due to inclusion of flexibility in the force field affect the way in which the molecules pack and thus will affect the predicted density of the crystal.

Panels a−c in Figure 2 respectively show the variation of ζ, number density ρ, and the energy per molecule E, as functions of the simulation time step n_s for an ideal TNAZ lattice (i.e., no voids) initially equilibrated at $P = 1$ atm and $T_0 = 440$ K. These curves show that the rapid jumps in ζ, ρ, and E occur at the time step that corresponds to the phase transition at 465 K.

Figure 3 gives the variation of the calculated melting temperature as a function of the number of voids n. Those values of n for which there are multiple transition temperatures

TABLE 4: Molecular Structural Parameters Describing Orientation[a] of the NO_2 Groups and Planarity of the Ring for the Eight TNAZ Molecules in the Unit Cell[d]

	1			2			3			4		
	expt[b]	NPTMD[c]		expt[b]	NPTMD[c]		expt[b]	NPTMD[c]		expt[b]	NPTMD[c]	
τ_1	166.4	172.8	(6.4)	166.4	172.9	(6.5)	166.4	173.0	(6.6)	166.4	172.9	(6.5)
τ_2	189.2	192.6	(3.4)	189.2	192.6	(3.4)	189.2	192.7	(3.5)	189.2	192.7	(3.5)
τ_3	−3.3	−4.8	(−1.5)	−3.3	−4.7	(−1.4)	−3.3	−5.4	(−2.1)	−3.3	−5.2	(−1.9)
τ_4	−0.1	25.0	(25.1)	−0.1	12.9	(13.0)	−0.1	0.9	(1.0)	−0.1	15.7	(15.8)
τ_5	−0.1	−10.9	(−10.8)	−0.1	−11.2	(−11.1)	−0.1	4.6	(4.7)	−0.1	−11.1	(−11.0)
τ_6	161.6	155.0	(−6.6)	161.6	154.9	(−6.7)	161.6	154.8	(−6.8)	161.6	155.0	(−6.6)
τ_7	223.6	220.0	(−3.6)	223.6	219.9	(−3.7)	223.6	219.8	(−3.8)	223.6	219.9	(−3.7)
	5			6			7			8		
	expt[b]	NPTMD[c]		expt[b]	NPTMD[c]		expt[b]	NPTMD[c]		expt[b]	NPTMD[c]	
τ_1	193.6	186.7	(−6.9)	193.6	187.0	(−6.6)	193.6	186.9	(−6.7)	193.6	187.0	(−6.6)
τ_2	170.8	167.4	(−3.4)	170.8	167.3	(−3.5)	170.8	167.6	(−3.2)	170.8	167.2	(−3.6)
τ_3	3.3	4.8	(1.5)	3.3	4.6	(1.3)	3.3	5.0	(1.7)	3.3	4.7	(1.4)
τ_4	0.1	−3.1	(−3.2)	0.1	−6.6	(−6.7)	0.1	0.8	(0.7)	0.1	−6.1	(−6.2)
τ_5	0.1	10.8	(10.7)	0.1	10.9	(10.8)	0.1	10.5	(10.4)	0.1	11.2	(11.1)
τ_6	198.4	205.5	(7.1)	198.4	205.2	(6.8)	198.4	205.3	(6.9)	198.4	205.2	(6.8)
τ_7	136.4	140.5	(4.1)	136.4	140.2	(3.8)	136.4	140.3	(3.9)	136.4	140.1	(3.7)

[a] Units are degrees. [b] Archibald et al., ref 20. [c] Values in parentheses are absolute differences from experimental values. [d] The NPTMD values are averaged over time and unit cells within the 4 × 2 × 2 simulation cell.

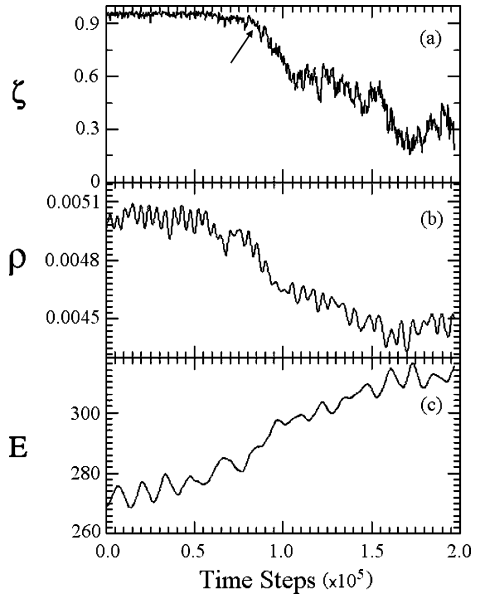

Figure 2. (a) Order parameter ζ, (b) number density ρ (in molecules/Å^3), and (c) energy per molecule E (in kJ/mol) as functions of the integration time steps (1 time step = 1 fs) for TNAZ; $P = 1$ atm, $T_0 = 440.0$ K, and $\Delta T = 2.5 \times 10^{-4}$ K. The arrow in frame a indicates the time when the melting starts.

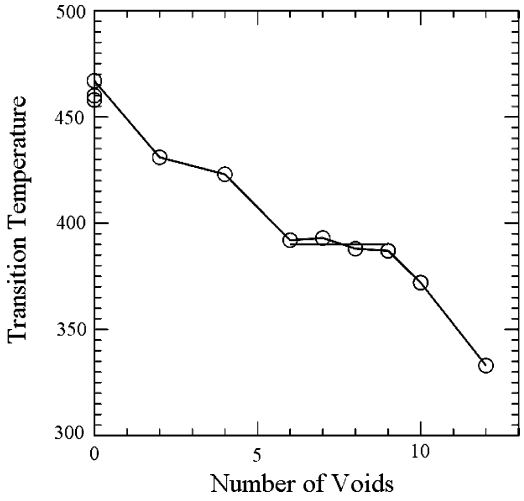

Figure 3. Calculated melting temperature T_m as a function of the number of voids n at $P = 1$ atm (open circles) for TNAZ. The predicted thermodynamic melting point, 390 K, is the average temperature in the plateau region (shown by the horizontal straight line).

demonstrate the effects due to varying either the initial phase or the initial temperature. The variation of the melting temperature with n as shown in the figure shows that the melting temperature decreases with increasing n until a plateau region is reached extending from $n = 6$ to 9. When the number of voids in the crystal is sufficiently large to render the structure unstable, the melting temperature drops abruptly. Solca et al.[27,28] assumed that the temperature in such a plateau region is the thermodynamic melting point. Agrawal et al.[29] also employed the same assumption to compute the melting points of Ar. Comparisons of the results of Agrawal et al.[29] for Ar with the computed thermodynamic results of Zha et al.[30] for the same potential energy surface over a wide range of pressure supports the validity of this assumption. A similar agreement[6] of the void-nucleated melting results with those given by the simulation of coexisting liquid and solid phases on nitromethane also supports the validity of the assumption that the melting point in the plateau region is the thermodynamic melting point. Following the same assumption and by averaging the melting temperature data in the plateau region, we obtain a melting point of 390 K, ∼4% higher than the experimental melting temperature[3] for TNAZ.

The isotherm of TNAZ at 300 K is shown in Figure 4. The values of B_0 and B_0', calculated by fitting the isotherm to the Birch−Murnaghan equation of state, are 5.93 GPa and 14.9, respectively. To our knowledge, there are no experimental data for these properties of TNAZ.

V. Conclusions

Two fully flexible force fields have been employed to study several fundamental physical properties of TNAZ with molecular dynamics simulations. One is the Generalized AMBER (GAFF)[1] force field and the other is a combination of the AMBER intramolecular force field and the Sorescu−Rice−Thompson intermolecular force field.[5] We have compared the calculated density, crystal lattice parameters, molecular and

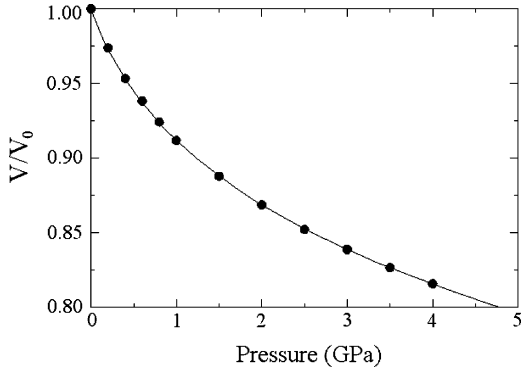

Figure 4. The calculated isotherm of crystalline TNAZ for the AMBER-SRT potential at 300 K. The volume of the simulation cell, V, divided by the volume at 1 atm, V_0, computed at fixed values of pressure (shown by the points) was fit to the Birch−Murnaghan equation (eq 6), and is shown by the curve.

crystal structures, and melting point with experimental values. The calculated thermodynamic melting point from the AMBER-SRT potential is 390 K, in good agreement with experiment (about 4% higher), while the AMBER potential predicts a T_m of 462 K. Comparison with experiment shows that both force fields predict a density of crystalline TNAZ that is about 10% smaller than the measured one. The calculated crystal lattice parameters from the AMBER-SRT potential are within ∼5% of the experimental values. Detailed studies on the calculated molecular structures and their arrangement within the predicted unit cell show that crystalline and molecular structural properties are well conserved with use of the AMBER-SRT potential. Finally, we predicted the isotherm of TNAZ up to 4 GPa and calculated the bulk modulus and its pressure derivative to be 5.93 GPa and 14.9, respectively. Overall, the proposed AMBER-SRT force field performs better than the AMBER force field, gives reasonably good results in predicting the physical properties of TNAZ, and provides valuable information on seeking a more accurate force field.

Acknowledgment. The authors thank Dr. Dan C. Sorescu for several fruitful discussions and suggestions. This work was supported in part by a DOD MURI grant managed by the Army Research Office.

References and Notes

(1) Case, D. A.; Pearlman, D. A.; Caldwell, J. W.; Cheatham, T. E., III; Wang, J.; Ross, W. S.; Simmerling, C. L.; Darden, T. A.; Merz, K. M.; Stanton, R. V.; Cheng, A. L.; Vincent, J. J.; Crowley, M.; Tsui, V.; Gohlke, H.; Radmer, R. J.; Duan, Y.; Pitera, J.; Massova, I.; Seibel, G. L.; Singh, U. C.; P, Weiner, K.; Kollman, P. A., Eds. *AMBER 7*; University of California, 2002.

(2) Oyumi, O.; Brill, T. B. *Combust. Flame* **1985**, *62*, 225.

(3) Sikder, N.; Sikder, A. K.; Bulakh, N. R.; Gandhe, B. R. *J. Hazard. Mater.* **2004**, *113*, 35.

(4) Thompson, C. A.; Rice, J. K.; Russell, T. P.; Seminario, J. M.; Politzer, P. *J. Phys. Chem. A* **1997**, *101*, 7742.

(5) Sorescu, D. C.; Rice, B. M.; Thompson, D. L. *J. Phys. Chem. B* **1997**, *101*, 798.

(6) Agrawal, P. M.; Rice, B. M.; Thompson, D. L. *J. Chem. Phys.* **2003**, *119*, 9617.

(7) Velardez, G. F.; Alavi, S.; Thompson, D. L. *J. Chem. Phys.* **2003**, *119*, 6698.

(8) Velardez, G. F.; Alavi, S.; Thompson, D. L. *J. Chem. Phys.* **2004**, *120*, 9151.

(9) Alavi, S.; Thompson, D. L. *J. Chem. Phys.* **2005**, *122*, 154704.

(10) Alavi, S.; Thompson, D. L. *J. Phys. Chem. B* **2005**, *109*, 18127.

(11) Zheng, L.; Thompson, D. L. To be submitted for publication.

(12) Sorescu, D. C.; Rice, B. M.; Thompson, D. L. *J. Phys. Chem. B* **2000**, *104*, 8406.

(13) Jorgensen, W. L.; Maxwell, D. S.; Tirado-Rives, J. *J. Am. Chem. Soc.* **1996**, *118*, 11225.

(14) Sorescu, D. C.; Rice, B. M.; Thompson, D. L. *J. Phys. Chem. B* **1998**, *102*, 8386.

(15) Sorescu, D. C.; Rice, B. M.; Thompson, D. L. *J. Phys. Chem. B* **1999**, *103*, 6783.

(16) Sorescu, D. C.; Rice, B. M.; Thompson, D. L. *J. Phys. Chem. B* **2001**, *105*, 9336 2001.

(17) Sorescu, D. C.; Thompson, D. L. *J. Phys. Chem. A* **2001**, *105*, 720.

(18) Breneman, C. M.; Wiberg, K. B. *J. Comput. Chem.* **1990**, *11*, 361.

(19) Frisch, M. J.; Trucks, G. W.; Schlegel, H. B.; Gill, P. M. W.; Johnson, B. G.; Robb, M. A.; Cheeseman, J. R.; Keith, T.; Patersson, G. A.; Montgomery, J. A.; Raghavachari, K.; Al-Laham, M. A.; Zakrzewski, V. G.; Ortiz, J. V.; Foresman, J. B.; Cioslowski, J.; Stefanov, B. B.; Nanyakkara, A.; Challacombe, M.; Peng, C. Y.; Ayala, P. Y.; Chen, W.; Wong, M. W.; Andres, J. L.; Replogle, E. S.; Gomperts, R.; Martin, R. L.; Fox, D. J.; Binkley, J. S.; Defrees, D. J.; Baker, J.; Stewart, J. P.; Head-Gordon, M.; Gonzales, C.; Pople, J. A. *GAUSSIAN 98*, Revision A.7,; Gaussian, Inc.: Pittsburgh, PA, 2001.

(20) Archibald, T. G.; Gilardi, R.; Baum, K.; George, C. *J. Org. Chem.* **1990**, *55*, 2920.

(21) Melchionna, S.; Ciccotti, G.; Holian, B. L. *Mol. Phys.* **1993**, *78*, 533.

(22) Allen, M. P.; Tildesley, D. J. *Computer Simulation of Liquids*; Oxford Science Publications: Oxford, UK, 1993.

(23) Forester, T. R.; Smith, W., Ed., *DLPOLY 2.10*; CCLRC, Daresbury Laboratory: Cheshire, UK, 1995.

(24) Ewald, P. *Ann. Phys.* **1921**, *64*, 253.

(25) Birch, F. *Phys. Rev.* **1947**, *71*, 809.

(26) Rice, B. M.; Sorescu, D. C. *J. Chem. Phys. B* **2004**, *108*, 17730.

(27) Solca, J.; Dyson, A. J.; Steinebrunner, G.; Kirchner, B. *Chem. Phys.* **1997**, *224*, 253.

(28) Solca, J.; Dyson, A. J.; Steinebrunner, G.; Kirchner, B.; Huber, H. *J. Chem. Phys.* **1998**, *108*, 4107.

(29) Agrawal, P. M.; Rice, B. M.; Thompson, D. L. *J. Chem. Phys.* **2003**, *118*, 9680.

(30) Zha, C.-S.; Boehler, R.; Young, D. A.; Ross, M. *J. Chem. Phys.* **1986**, *85*, 1034.